Estelle Deboever ORCID iD: 0000-0001-5707-9483

Modulation of Plant Plasma Membrane Structure by Exogenous Fatty Acid Hydroperoxide is a Potential Perception Mechanism for their Eliciting Activity

DEBOEVER Estelle [1,2,8], VAN AUBEL Géraldine [3,8], RONDELLI Valeria [4], KOUTSIOUMPAS Alexandros[5], MATHELIE-GUINLET Marion [6], DUFRENE Yves F. [6], ONGENA Marc [7], LINS Laurence [1], VAN CUTSEM Pierre [3,8], FAUCONNIER Marie-Laure [2*] and DELEU Magali [1*]

[1]Laboratory of Molecular Biophysics at Interfaces, Gembloux Agro-Bio Tech, University of Liège, 2, Passage des Déportés, B-5030 Gembloux, Belgium

[2]Laboratory of Natural Molecules Chemistry, Gembloux Agro-Bio Tech, University of Liège, 2, Passage des Déportés, B-5030 Gembloux, Belgium

[3]Research Unit in Plant Cellular and Molecular Biology, University of Namur, Rue de Bruxelles, 61, B-5000 Namur, Belgium

[4] Department of Medical Biotechnologies and Translational Medicine, Università degli Studi di Milano, L.I.T.A., Via F.lli Cervi 93, 20090 Segrate, Italy

[5]Jülich Centre for Neutron Science (JCNS) at Heinz Maier-Leibnitz Zentrum (MLZ), Forschungszentrum Jülich GmbH, Lichtenbergstrasse 1, 85748 Garching, Germany

[6]Institute of Biomolecular Science and Technology (IBST), Croix du sud 4-5/L7.07.06, B-1348 Louvain-la-Neuve, Belgium

[7]Microbial Processes and Interactions (MiPI), Gembloux Agro-Bio Tech, Université de Liège, 2, Passage des Déportés, B-5030 Gembloux, Belgium

[8]FytoFend S.A., rue Georges Legrand, 6, B-5032 Isnes, Belgium

*****Correspondence: magali.deleu@uliege.be (M.D.) + marie-laure.fauconnier@uliege.be (M-L. F.)

This article has been accepted for publication and undergone full peer review but has not been through the copyediting, typesetting, pagination and proofreading process, which may lead to differences between this version and the Version of Record. Please cite this article as doi: 10.1111/pce.14239.

Author email address: Deboever Estelle: e.deboever@fytofend.com; Van Aubel Géraldine: geraldine.vanaubel@unamur.be; Rondelli Valeria: valeria.rondelli@unimi.it; Koutsioumpas Alexandros: a.koutsioumpas@fz-juelich.de; Mathelie-Guinlet Marion: marion.mathelie@uclouvain.be; Dufrêne Yves: yves.dufrene@uclouvain.be; Ongena Marc: marc.ongena@uliege.be; Lins Laurence: l.lins@uliege.be; Van Cutsem Pierre: pierre.vancutsem@unamur.be; Fauconnier Marie-Laure: marie-laure.fauconnier@uliege.be; Deleu Magali: magali.deleu@uliege.be

Date of submission:

Number of Tables: 0 - Number of Figures: 5

Word count: 6178

Supplementary data: Figures: 3 - Tables: 2

Short Title: Plant hydroperoxide eliciting activity is linked to PPM modulation

Highlight: Modulation of the lipid dynamics of plant plasma membrane by exogenous fatty acid hydroperoxide oxylipins triggers early defence events like ROS production leading to plant resistance against pathogens

Abstract: Oxylipins are lipid-derived molecules that are ubiquitous in eukaryotes and whose functions in plant physiology have been widely reported. They appear to play a major role in plant immunity by orchestrating reactive oxygen species (ROS) and hormone-dependent signalling pathways. The present work focuses on the specific case of fatty acid hydroperoxides (HPOs). Although some studies report their potential use as exogenous biocontrol agents for plant protection, evaluation of their efficiency *in planta* is lacking and no information is available about their mechanism of action. In this work, the potential of 13(*S*)-hydroperoxy-(9*Z*,11*E*)-octadecadienoic acid (13-HPOD) and 13(*S*)-hydroperoxy-(9*Z*,11*E*,15*Z*)-octadecatrienoic acid (13-HPOT), as plant defence elicitors and the underlying mechanism of action are investigated. *Arabidopsis thaliana* leaf resistance to *Botrytis cinerea* was observed after root application with HPOs. They also activate early immunity-related defence responses, like ROS. As previous studies have demonstrated their ability to interact with plant plasma membranes (PPM), we have further investigated the effects of HPOs on biomimetic PPM structure using complementary biophysics tools. Results show that HPO insertion into PPM impacts its global structure without solubilizing it. Relationship between biological assays and biophysical analysis suggests that lipid amphiphilic elicitors that directly act on membrane lipids might trigger early plant defence events.

Graphical Abstract

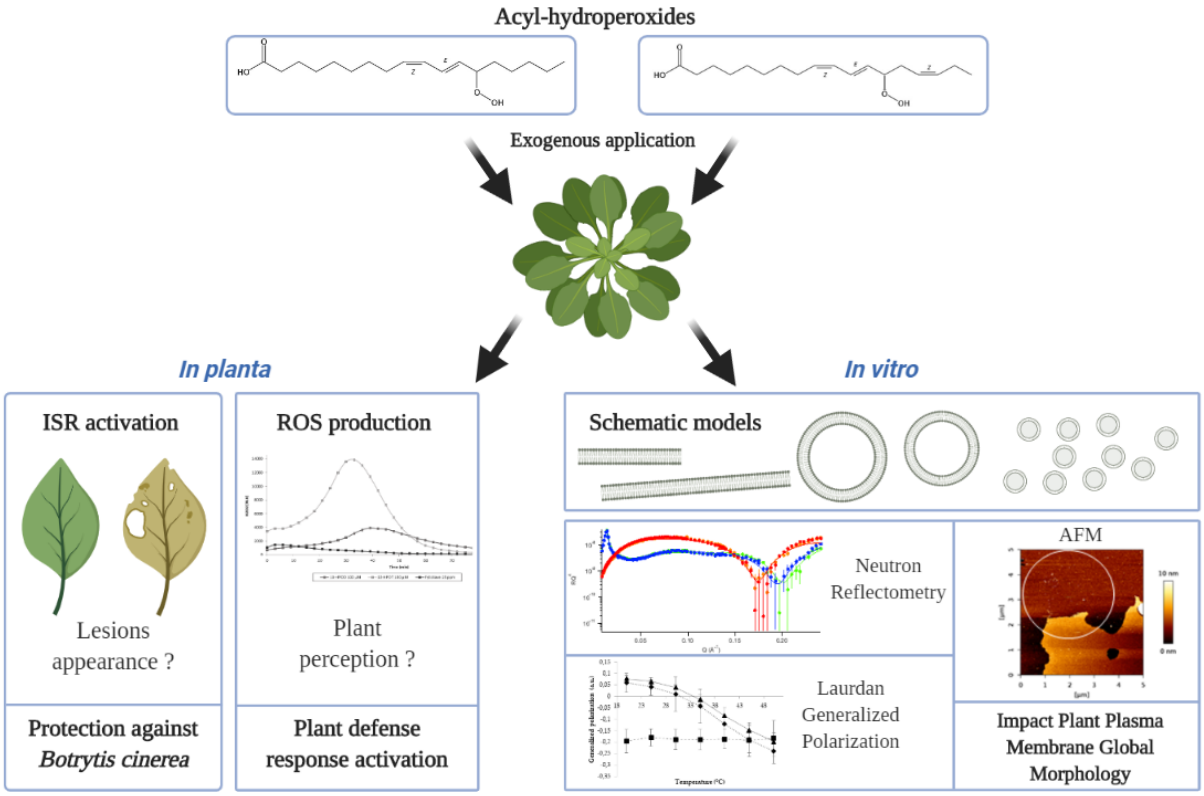

Keywords: Elicitor, Fatty Acid Hydroperoxide, Molecular Mechanism, Oxidative Burst, Oxylipin, Plant Defence, Plant Plasma Membrane.

Abbreviations: (13-HPOD) 13-hydroperoxy- 9,11-octadecadienoic acid; (13-HPOT) 13-hydroperoxy- 9,11,15-octadecatrienoic acid; (AFM) atomic force microscopy; (CMC) critical micelle concentration; (COS) chitooligosaccharides, (d_{62}DPPC) 1,2-dipalmitoyl-d62-sn-glycero-3-phosphocholine; (DAMP) damage-associated molecular pattern; (DMSO) dimethylsulfoxide; (Flg22) flagellin; (GIPC) glycosyl-inositol-phosphoryl-ceramide; (GluCer) glucosylceramide; (GP) generalized polarization; (HPO) fatty acid hydroperoxide; (ISR) induced systemic resistance; (LOX-1) Lipoxidase from Glycine max (soybean) type I-B; (MLV) multilamellar vesicles; (MS) Murashige and Skoog medium; (NR) neutron reflectometry; (OGA) oligogalacturonides; (PAMP) pathogen-associated molecular pattern; (PLPC) 1-palmitoyl-2-linoleoyl-sn-glycero-3-phosphocholine; (POX) peroxidase; (PPM) plant plasma membrane; (PRR) pattern recognition receptor; (RBOH) respiratory burst oxidase homolog; (RLU) relative light unit; (ROS) reactive oxygen species, (RL)

rhamnolipid, (RT) room temperature; (SR) systemic resistance; (SAR) systemic acquired resistance; (SLB) supported lipid bilayer; (SLD) scattering length density; (SUV) small unilamellar vesicle; (THSD) Tukey honest significant differences; (TRIS) tri(hydroxymethyl)aminomethane.

1 Introduction

Since several chemical pesticides have been shown to be detrimental on human health and ecosystems, considerable research has been done to find more environment-friendly plant protection solutions (Gay, 2012; Hernández *et al.*, 2013; Wang *et al.*, 2013; Carvalho, 2017). Elicitors, defined as molecules able to stimulate defence responses in a host plant, are one of the emerging alternatives (Paré *et al.*, 2005; Henry *et al.*, 2012; Thakur and Sohal, 2013). They can be derived from plants (termed as Damage-Associated Molecular Patterns (DAMPs)) or microorganisms (referred as Microbe-Associated Molecular Patterns (MAMPs) or Pathogen-Associated Molecular Patterns (PAMPs)) (Yu *et al.*, 2017; Malik *et al.*, 2020; Nishad *et al.*, 2020; Ngou *et al.*, 2021*b*; Song *et al.*, 2021). For example, flagellin (flg22) or cryptogein are a bacterial and a fungal elicitor respectively (Gómez-Gómez and Boller, 2002; Gerbeau-Pissot *et al.*, 2014). Chemically synthesized molecules like rhamnolipid bolaforms and bio-based molecules like COS-OGA can also act as elicitors (Clinckemaillie *et al.*, 2017; Luzuriaga-Loaiza *et al.*, 2018). Elicitors can hence be of different chemical natures like carbohydrate polymers, lipids, peptides or proteins (Boller and Felix, 2009; Thakur and Sohal, 2013; Jogaiah *et al.*, 2019; Pršić and Ongena, 2020).

Recognition of elicitors by the plant cells first triggers early defence responses among which the release of reactive oxygen species (ROS) (superoxide anion ($O_2^{\bullet -}$), hydrogen peroxide (H_2O_2) and hydroxyl radical ($^{\bullet}OH$)), also known as the oxidative burst (Mittler, 2017; Shang-Guan *et al.*, 2018; Camejo *et al.*, 2019; Zaid and Wani, 2019). The perception of elicitors by plant cells further results in protection based on the activation of signalling cascades and defence mechanisms leading to the induction of plant immunity, like the

systemic acquired resistance (SAR) and the induced systemic resistance (ISR) (Malik *et al.*, 2020; Pršić and Ongena, 2020).

In addition to be a selective barrier between the cell and the extracellular medium, the plasma membrane is a sensor for modification of cellular environment and plays thus a key role in the recognition process of bioactive molecules. While most of elicitors are perceived by membrane proteic receptors, the involvement of the lipid part of the cell membrane has not been ruled out (Nimchuk *et al.*, 2003; Deleu *et al.*, 2019). Indeed, many danger signals or invasion patterns are recognized by specific pattern recognition receptors within PPM (Schellenberger *et al.*, 2019; Pršić and Ongena, 2020), and some amphiphilic elicitors, like surfactin from *Bacillus* and rhamnolipids (RLs) from *Pseudomonas*, have been strongly suggested to be perceived by the lipid fraction of PPM (Henry *et al.*, 2011; Gerbeau-Pissot *et al.*, 2014; Haba *et al.*, 2014; Luzuriaga-Loaiza *et al.*, 2018; Monnier *et al.*, 2018; Herzog *et al.*, 2020; Come *et al.*, 2021). Very recently, it was also demonstrated that the RL-triggered immune response is independent of the LORE receptor and is affected by the sphingolipid composition of the plasma membrane suggesting a direct interaction of RLs with plant plasma membrane lipids (Schellenberger *et al.*, 2021), similar to what has been shown on membrane models (Luzuriaga-Loaiza *et al.*, 2018).

Fatty acid hydroperoxides (HPOs) are amphiphilic molecules naturally produced by plants in response to (a)biotic stresses by the oxidative catabolism of polyunsaturated fatty acids. They belong to the large family of plant oxylipins (Blée, 2002; Wasternack and Feussner, 2018; Genva *et al.*, 2019). Oxylipins are ubiquitous in the plant kingdom and can either be esterified, notably in biological membranes, or be found in free form. Among them, the best known are the jasmonates, a family of molecules including jasmonic acid (JA), its derivatives and some JA precursors such as 12-oxo-phytodienoic acid (OPDA) and 12-dinor-oxo-phytodienoic acid (dnOPDA) (Wasternack and Strnad, 2018). JA is obtained from 13-hydroperoxy-9,11,15-octadecatrienoic acid (13-HPOT) following the successive action of various enzymes (lipoxygenase, etc.) (Deboever *et al.*, 2020). 13-HPOT and its dienoic equivalent, 13-hydroperoxy-9,11-octadecadienoic acid (13-HPOD), are key intermediates in

the synthesis of jasmonates and other oxylipins, and have been extensively studied for their signalling properties (Deboever *et al.*, 2020). In the recent years, HPOs have emerged as a promising plant defence solution and their exogenous application to protect plants against phytopathogens has been considered (Granér *et al.*, 2003; Prost *et al.*, 2005; Deboever *et al.*, 2020). However, their biological activities in plant defense and hence their potential as elicitors still remain elusive. In addition, in our previous study (Deleu *et al.*, 2019), we have shown that HPOs are able to interact with PPM lipids inducing a perturbation of their lateral organization. We have suggested that, by this interaction, HPOs could activate cellular signaling involved in plant defense mechanisms.

In the present study, we first explored the potential of exogenously applied HPOs to protect *Arabidopsis thaliana* plants against *Botrytis cinerea* by a systemic signalling mechanism. Their eliciting activity was evaluated by measuring ROS production by *Arabidopsis thaliana* cells in their presence. In a second part, the molecular mechanism of HPO perception by the PPM was further investigated on plant biomimetic lipid systems by using a panel of complementary biophysical tools. More particularly, we analysed the effects of HPOs on the transversal organization and on the structure of the PPM bilayer.

The relationship between the results of biological assays and the effect of HPOs on model plant plasma membrane suggests that their action on the lipids might trigger early plant defence events.

2 Experimental procedures

2.1 Materials

As described in our previous works (Fauconnier and Marlier, 1996; Deleu *et al.*, 2019; Deboever *et al.*, 2020), HPOs were enzymatically synthetized from the reaction of LOX-1 on linoleic (13-HPOD) or linolenic acid (13-HPOT). The purity (higher than 98%) was checked by high-performance liquid chromatography. For deuterated 13-HPOD, we used

only deuterated reactants and solvents. Nuclear magnetic resonance and mass spectrometry were used for a full chemical characterization of the samples (data not shown).

1-palmitoyl-2-linoleoyl-sn-glycero-3-phosphocholine (PLPC), β-sitosterol, C16 glucosyl(ß) ceramide (d18:1/16:0) (GluCer), lipoxidase from *Glycine max* (soybean) type I-B (LOX-1), the linoleic and α- linolenic acids, 6-Dodecanoyl-N,N-dimethyl-2-naphthylamine (Laurdan), horseradish peroxidases, luminol were purchased from Sigma-Aldrich (Belgium). 1,2-dipalmitoyl-d62-sn-glycero-3-phosphocholine (d_{62}DPPC) was purchased from Avanti Polar Lipids (Italy). Deuterium oxide (D_2O) of 99.8% purity was purchased from ARMAR (Europa) GmbH. Chloroform and methanol were both purchased from Scharlau Lab Co. Dimethylsulfoxide (DMSO) and tri(hydroxymethyl)aminomethane (TRIS) were provided by Sigma Chemical. The ultrapure water was produced by Millipore systems available in our laboratory, the resistivity was 18.2 MΩ cm. The active substance COS-OGA was provided by FytoFend S.A. (Belgium) under the composition FytoSave® (12.5 g/L COS-OGA). *Botrytis cinerea* was grown on oat-based medium (25 g/L oat flour, 12 g/L agar) at room temperature.

2.2 Induction of systemic resistance

2.2.1 In *Arabidopsis thaliana* seedlings

The capacity of HPOs to trigger systemic resistance (SR) was tested on *A. thaliana* infected by *B. cinerea* according to the procedure described in (Ongena *et al.*, 2000). HPOs were applied on the root system and the bacteria were inoculated on the leaves in order to assess the systemicity of the response. Seeds were sterilized with ethanol (70% v/v) and bleach (15% v/v) before multiple rinsing with sterile water, sowed in a square Petri Dish filled with agar medium (6-8 g/L) and transferred to a growth room at 22°C under a 16 h light/8 h dark photoperiod. After one week, seedlings were transferred to a sterile Araponics system filled with hydroponic solution (5 mL/10 L of Hydroponic Nutrient Solution 3-part Mix). After approximately 5 weeks in the growth room, the plants were transferred to 10 mL vials containing 10 mL hydroponic and kept in the dark wrapped in aluminium foil then transferred to adapt for one day before elicitation. The next day, half of the plant roots were treated in

vials with 10 mL hydroponic solution supplemented with 20 mM HPOs in 1% DMSO. The other half (control) was treated with 10 mL hydroponic solution with 1% DMSO. After 24 h, four leaves of each plant were infected with *B. cinerea*. A 3-µL droplet containing 2 500 spores was deposited on the adaxial face of each leaf. Four days after inoculation, the disease was scored as the percentage of *B. cinerea* lesions having extended beyond the inoculum drop zone to produce spreading lesions (Ongena *et al.*, 2000, 2007). Three independent experiments were carried out, with 8 plants per treatment (n=24).

2.3 Production of H_2O_2 by *Arabidopsis thaliana*

2.3.1 On plant cell suspensions

Photoautotrophic cell suspensions from *A. thaliana* ecotype Landsberg ecotype were cultured on a rotary shaker at 100 rpm, in Murashige and Skoog (MS) medium (4.4 g/L) with 0.5 mg/L naphthalene acetic acid, 0.05 mg/L kinetin, pH 5.7 and maintained at 24°C with approximately 2% CO_2 under a 16 h/8 h light/dark photoperiod. H_2O_2 production was assessed using luminol-dependent chemiluminescence on seven-day-old cells directly after the addition of the elicitors in the growth medium, according to the method described by Baker and Mock (Baker and Mock, 2004). Luminescence (relative light units, (RLU)) was measured every three min for 90 min. Eight technical replicates were carried out for each test compound and three independent measurements were performed (n=24). Results were expressed as means ± standard deviations of the area under the H_2O_2 production curves. ROS production values were analysed using Tukey Honest Significant Differences (THSD) test for multiple comparisons (p values < 0.1).

2.3.2 On foliar discs

A. thaliana plants were grown as described by Smith and Heese (Smith and Heese, 2014). For all ROS experiments, measurements were performed on 5-mm disks prepared from leaves from 4-week old plants using a method adapted from Smith and Heese (Smith and Heese, 2014). The day before the experiment, disks were placed in water in a 96 wells plate. The day of measurements, the water was replaced by 150 µL of treatment solutions (20

µg/mL horseradish POX, 0.2 mM luminol and HPO) including test compounds. Luminescence (RLU) was monitored every 3 min for 90 min. Two independent biological repetitions were obtained with six foliar disks each (6 technical replicates/treatment). Results were then expressed as means ± standard deviations (n = 12) of the area under the H_2O_2 production curves. ROS production values were analyzed using Tukey Honest Significant Differences (THSD) test for multiple comparisons ($p< 0.05$).

2.4 Calcein leakage

PLPC/sito/GluCer (60:20:20) small unilamellar vesicles (SUVs) were prepared as described previously (Deleu *et al.*, 2013, 2019; Deboever *et al.*, 2020). PLPC, sitosterol and GluCer in proportion 60:20:20 were dissolved in a chloroform/methanol mixture (2/1, v/v). The solvent was evaporated under a gentle stream of nitrogen to obtain a dried lipid film which was maintained under vacuum overnight. 10 mM calcein in 10 mM TRIS-HCl buffer pH 7.4 was added to hydrate the dried lipid film. The lipid dispersion was maintained at 37°C for at least 1 h and vortexed every 10 min. 5 cycles of freeze-thawing were applied to spontaneously form multilamellar vesicles. To obtain SUVs, this suspension was sonicated to clarity (5 cycles x 2 min) using a titanium probe with 400W amplitude keeping the suspension in an ice bath. Finally, generated titanium particles were removed from SUV solution by centrifuging during 10 min at 6200 rpm. The unencapsulated calcein was removed from the SUV dispersion by the Sephadex G65 mini-column separation technique (Fu and Singh, 1999). The actual phospholipid content of each preparation was determined by phosphorus assay (Bartlett, 1958) and the concentration of liposomes was adjusted for each type of experiment to 5 µM in 10 mM TRIS-HCl buffer at pH 7.4.

Fluorescence was measured as previously described in (Bartlett, 1958) with a Perkin Elmer (model LS50B) fluorescence spectrometer equipped with polarizers. Total amount of calcein release was determined by adding Triton-X100 (0.2%) to a liposome suspension that dissolved the lipid membrane without interfering with the fluorescence signals. The emission and excitation wavelengths were set at 517 nm and 467 nm, respectively. A fluorescence

signal of 750 µL of SUV was first recorded as a baseline, followed by the addition of 13-HPOD/T (at t=30 sec) in 7 different concentrations while continuing the recording for 900 s. The amount of calcein released after time t was calculated according to (Shimanouchi *et al.*, 2009):

$$RF\ (\%) = 100\ \frac{(I_t - I_o)}{(I_{max} - I_o)}$$

where RF is the fraction of calcein released, I_o, I_t and I_{max} are the fluorescence intensities measured at the beginning of the experiment, at time t and after the addition of 0.2% Triton X-100, respectively. All experiments were carried out at least three times, each time with freshly prepared SUVs.

2.5 Laurdan generalized polarization

For Laurdan generalized polarization experiments, multilamellar vesicles (MLVs) were prepared based on (Parasassi and Gratton, 1995; Deboever *et al.*, 2020). PLPC, sitosterol and GluCer in proportion 60:20:20 were dissolved in a chloroform/methanol mixture (2/1, v/v). HPOs were added to the lipid mixture to reach a lipid:HPO molar ratio of 5:1. The solvent was evaporated under a gentle stream of nitrogen to obtain a dried lipid film which was maintained under vacuum overnight. The resulting film was hydrated with 10 mM Tris-HCl buffer at pH 7.4 prepared from Milli-Q water and 1 µL of Laurdan solution prepared in DMSO was added to reach a final concentration of 5 nM. The lipid dispersion was maintained at a temperature well above the transition phase temperature of the lipid for at least 1 h and vortexed every 10 min.

Fluorescence of Laurdan in MLVs was monitored at various temperatures (between 20 and 50°C by steps of 5°C) with a Perkin Elmer LS50B fluorescence spectrometer. Samples were placed in 10 mm pathlength quartz cuvettes under continuous stirring and the cuvette holder was thermostated with a circulating bath. Samples were equilibrated at each temperature for 10-15 min prior to the measurements.

The excitation wavelength was set to 360 nm (slit = 2.5 nm), and at least 10 measurements of emission intensities at 440 nm and 490 nm were recorded and averaged for

each sample and the blank (DMSO) at each temperature. An emission spectrum from 400 nm to 600 nm (slit = 4.5 nm) was also recorded for each sample-temperature combination. Generalized polarization (GP) of Laurdan was then calculated according to (Parasassi *et al.*, 1992; Harris *et al.*, 2002):

$$GP = \frac{I_{440} - I_{490}}{I_{440} + I_{490}}$$

where I_{440} and I_{490} are the blank-subtracted emission intensities at 440 nm and 490 nm, respectively. All experiments were carried out at least three times, each time with freshly prepared MLVs.

2.6 Neutron reflectometry

Neutron reflectometry (NR) measurements were performed at the MARIA neutron reflectometer (Mattauch *et al.*, 2018) operated by Jülich Centre for Neutron Science at Heinz Maier-Leibnitz Zentrum in Garching (Germany) while using custom temperature-regulated (through a connected Julabo F12-ED circulator) liquid cells (Koutsioubas, 2016). Two different wavelengths were used, 10 Å for the low-q region and 5 Å for the high-q region, and the reflected intensity has been collected at different angles, up to 0.25 $Å^{-1}$ q values, with a 10% wavelength spread. Using a peristaltic pump combined with valves (flow rate ~0.5 mL/min) solvent exchange was possible without moving the measuring cells from the instrument.

Specular NR measures the thickness and scattering length density (SLD) profile of layered structures along the surface normal (z). The SLD distribution along the normal, represented as ρ(z), is specific of the chemical composition of materials along the normal and depends on the coherent nuclear scattering lengths (b_i) of its constituent atoms and their number density along the normal (n_i (z)) so that $\rho(z) = \sum_i b_i n_i (z)$. In reflectivity data measurements, the intensity of reflected neutrons is recorded relatively to the incident beam as a function of the momentum transfer vector ($q = 4\pi\sin\theta/\lambda$), where θ is the incidence angle and λ the wavelength of incident neutrons. The variation of reflectivity as a function of

momentum transfer $R(q_z)$ is related to the square modulus of the one-dimensional Fourier transform of the SLD profile along the normal to the interface ($\rho(q_z)$) through the relation:

$$R(q_z) \sim (16\pi^2 / {q_z}^2)|\rho(q_z)|^2$$

Following the characterization by neutron reflectivity of silicon/solution interface, we deposited by vesicle fusion the membrane of interest (Koutsioubas *et al.*, 2017). After its full characterization in 150 mM NaCl solutions in D_2O and H_2O, 2 µg of 13-HPOD/T, deuterated or not depending on the membrane studied, were injected in the measuring cell (6 mL total volume), to a final concentration lower than their critical micelle concentration (CMC = 25.4 ± 1.9 µM and 24.0 ± 1.3 µM for 13-HPOT and 13-HPOD, respectively, according to (Deleu *et al.*, 2019). Reflectivity was measured after letting the systems equilibrate for 1 h, again in the two contrasts condition with 10 mM Tris (pH 7.4).

To analyse the specular reflection data, the interface is modelled as a series of parallel layers where each layer is characterized by an average SLD and a thickness. Based on these parameters, a model reflectivity profile is calculated by means of the optical matrix method (Névot and Croce, 1980). The interfacial roughness between two consecutive layers is included in the model by the Abeles method, as described by Nevot and Croce (Névot and Croce, 1980).

Finally, the calculated model profile is compared to the measured profile and the quality of the fit is assessed by using the χ^2 in minimum-squares method. In this way, fittings are optimized on the basis of the minimal χ^2 reached. Errors on parameters values have been estimated from the maximum variation in the acceptable fit subject to the constraints of space filling and stoichiometry. NR is a technique suited to collect structural information about the different layers of the studied membrane (Rondelli *et al.*, 2019). Thus, the silicon support and the bulk water are seen as bulk infinite layer, the silicon oxide layer, the water layer between the silicon oxide and the membrane and the diverse hydrophilic/hydrophobic layers of the lipid membranes are modelled as defined layers with a proper thickness, roughness with respect to the previous layer, compactness, composition and consequently contrast. Supported lipid bilayers (SLB) were formed using both the same lipid mixture as previously

(PLPC/sito/GluCer in molar ratio 60/20/20) and d_{62}DPPC. Injections were done at 47°C and measurements at room temperature (RT). The reflectivity profile of the silicon support and of the samples has been measured in different contrasts (H_2O and D_2O) and data analysis was performed with the fit program MOTOFIT (Nelson, 2006). SLD used for the specific components are reported in Supplementary Data **Table S1**.

2.7 Atomic force microscopy

To probe the nanoscale effects of HPOs on lipid membranes, SLB (ternary mixture of PLPC/sito/GluCer (60/20/20)) were reconstructed on freshly cleaved mica substrates by allowing the fusion of a 2 mM lipid vesicles solution (V = 100 µL) at 55°C for 45 min. Samples were then left for thermalization at room temperature for 30 min without dewetting and immersed in 3 mL Tris buffer (pH 7.5).

To avoid damaging the samples, atomic force microscopy (AFM) images were obtained in the quantitative imaging (QI) mode of a JPK Nanowizard III setup, with a minimal applied force of 200 pN and a speed of 50 µm/s. Soft sharpened silicon nitride cantilevers (MSCT, Bruker) were used and calibrated before any experiment using the thermal noise method (k ~ 0.02 N/m). HPOs, prepared in Tris buffer, were injected to reach a final concentration of 3 µM below their critical micellar concentration. AFM images were then recorded at different time points in different areas to follow the HPOs impact on the lipid bilayer.

3 Results

3.1 *In planta* protective effect of HPOs against phytopathogens

The capacity of HPOs to induce SR in *A. thaliana* against *B. cinerea* was tested under controlled conditions by treating plant roots with HPO solutions and inoculating plant leaves with the pathogen. The disease severity with HPO treatment was measured after 4 days, compared to controls (treatment with water containing 1% DMSO) and we attributed a disease severity scores from 1 to 4 representing no symptoms (score 1) to full development of the

disease (score 4). Treatment with both HPOs provided similar obvious disease reduction as shown by the decreased size of the lesions (**Figure 1**). About 40% of the plants had no symptom which leads to disease severity scores mainly between 1 and 2.

Given the experimental design (treatment and infection on two different plant organs), this cannot be a direct biocidal effect but rather a systemic signalling in the plant. One can therefore wonder about the signalling mechanism initiated by HPOs and more particularly their initial perception by the plant cells and the responses they induce.

3.2 Perception of HPOs and early defenses responses activation

Very often, ROS production is a biphasic process with a first transient phase within minutes after the infection and a second more intense and sustained phase that can last for many hours (Shang-Guan *et al.*, 2018; Ngou *et al.*, 2021*a*). This first wave, which is linked to the activation of early defence responses, has been investigated to determine whether the two HPOs are perceived by plants and can induce an immune response.

Cell suspensions cultures are a valuable model system for studying elicitor-induced defence reactions in plants and they easily allow studying early signalling events like oxidative bursts (Khonon *et al.*, 2011; Jogaiah *et al.*, 2019). Here, photoautotrophic *A. thaliana* cell suspensions were used to detect H_2O_2 production after treatment with HPOs. ROS accumulation was detected using a luminol-based assay (van Aubel *et al.*, 2016; Monnier *et al.*, 2018). The elicitor FytoSave® was used as positive control as its active substance, COS-OGA made of pectin-derived oligogalacturonides (OGA) and chitooligosaccharides (COS) (Cabrera *et al.*, 2010), is known to induce a significant production of ROS at a concentration of 25 ppm (Ledoux *et al.*, 2014; van Aubel *et al.*, 2016). In our experiment, a range of six different concentrations (0.5 µM to 100 µM) was tested and ROS production was monitored for 90 min.

The ROS production after 13-HPOD or 13-HPOT treatment was concentration-dependent (**Figure 2A).** It was higher than the negative control but also higher than the positive control, for concentrations 50 µM and 100 µM. In those cases, the response to 13-

HPOT treatment is higher than the 13-HPOD one. Also, the oxidative burst peak occurred quicker (30 min instead of 40 min) for 13-HPOT than for 13-HPOD (**Figure 2B).** The same conclusion was drawn from experiments performed on foliar disks of *A. thaliana*, a plant model closer to the reality (see supplementary data – **Figure S1**).

Comparatively to COS-OGA, the kinetics of ROS production induced by HPOs in plant cells was slower (within 5 min only for COS-OGA *vs* 30-40 min for HPOs) but the oxidative burst lasted longer with a total duration of 60-70 min before returning to the basal level. Such long lasting response profile was also observed with synthetic RL bolaforms, for which it was suggested that their perception occurred via the lipid fraction of the plasma membrane (Bahar *et al.*, 2016; Luzuriaga-Loaiza *et al.*, 2018). On the contrary, the elicitor flg22, known to be perceived by membrane pattern recognition receptors (Meindl *et al.*, 2000; Smith and Heese, 2014), induces a quicker oxidative burst initiated within 4-6 min with a peak at ~10 min (Yu *et al.*, 2017), similarly to the OGA in the COS-OGA composition (Cabrera et al., 2008). Moreover, the induction of ROS production occurs at concentrations much higher than concentrations usually active when a proteic receptor is involved as for flg22 which still binds to its receptor at femtomolar concentrations (Meindl *et al.*, 2000; Zhao *et al.*, 2010).

The observation of different kinetic profiles and different concentration ranges for HPOs comparatively to classical elicitors would suggest that a proteic receptor is not directly involved in their recognition. Due to the ability of HPOs to interact with PPM lipids (Deleu *et al.*, 2019), we hypothesized that the HPOs would rather be recognized via the lipid phase of the membrane.

3.3 Changes of PPM biophysical properties induced by HPOs

The interaction of HPOs with PPM characteristic lipids has already been found to modify the lateral organization of membrane bilayer in terms of lipid domain size and distribution (Deleu *et al.*, 2019). It is also known that the plant sphingolipid GluCer is a

privileged partner for the interaction and that 13-HPOT has a higher interaction affinity than 13-HPOD.

In the present study, further analysis of the effects of HPOs interaction with lipids on PPM structure was carried out. Simplified biomimetic models with two different lipid compositions were studied, the first mimicking the PPM, namely PLPC:sito:GluCer (60/20/20), and the second made of d_{62}DPPC, a classic deuterated model.

3.3.1 Effect of HPOs on membrane permeability

First, we have investigated the ability of HPOs to permeabilize model membranes by measuring the release of calcein. If the membrane is permeabilized by a bioactive molecule, the self-quenched calcein initially encapsulated within the LUV is released into the external medium and gives rise to an increase of fluorescence emission. Very little permeabilization effect was observed (values less than 10%) for both HPOs on the PLPC:sito:GluCer membrane model (**Figure S2**) suggesting that HPOs would not derive their mode of action from a mechanism of solubilization of the membrane or pore formation, but rather a more subtle modification of the membrane organization that could lead to the activation of a signalling cascade.

3.3.2 Change in bilayer fluidity induced by HPOs

The effect of HPOs on the bilayer fluidity was investigated by monitoring the lipid phase-dependent emission spectrum shift of Laurdan, a fluorescent probe that readily locates at the hydrophilic/hydrophobic interface of bilayers (Harris *et al.*, 2002; Sanchez *et al.*, 2007). Its fluorescence depends on the physical state of the environment. When present in a gel phase bilayer, its maximum fluorescence intensity is close to 440 nm emission wavelength. When the bilayer is in a fluid state, the Laurdan maximum fluorescence is observed at higher wavelengths (around 490 nm). This "red-shift" phenomenon is due to a higher quantity and mobility of the water molecules located around the probe. This is directly related to the lower order within the bilayer and is measured by the Generalized Polarization (GP): a decreasing GP value corresponds to a higher fluidity of the bilayer (Parasassi *et al.*, 1991). This method

has been previously applied for investigating the effect of drugs, natural herbicides or other elicitors on lipid membrane organization (Deleu *et al.*, 2013; Sautrey *et al.*, 2014; Lebecque *et al.*, 2019; Furlan *et al.*, 2020).

The effect of HPOs on PLPC:sito:GluCer MLV membrane fluidity was investigated for a range of temperatures from 20°C to 50°C (**Figure 3**). In presence of 13-HPOT, the Laurdan GP values decreased significantly compared to those observed on pure MLVs with no significant effect of temperature. This indicates a fluidifying effect of 13-HPOT on the bilayer. On the contrary, 13-HPOD did not induce significant change in lipid order at any temperature as its curve almost superimposes to that of pure PLPC:sito:GluCer vesicles.

3.3.3 Effect of HPOs on the bilayer transversal structure

The effect of HPOs on the transversal structure of PPM was analysed by NR, a technique of choice to study the transverse structure of layered samples within a few Å resolution (Mattauch *et al.*, 2018) and to evidence the structural effects of the interaction of incoming molecules on biological membranes (Rondelli *et al.*, 2016, 2018). Neutrons interaction with matter depends on the isotopic species. Therefore, neutron-based experiments can profit by the use of deuterated molecules to enhance the visibility of molecules within a mixed complex system. As the lipids representative of the PPM are not commercially available in their deuterated form, d_{62}DPPC was used to form SLB and to highlight the presence and location of the H-bringing HPOs within the membrane. **Figure 4A-D** show the reflectivity curves together with their fittings in two contrasts and the corresponding fit parameters are summarized in **Figure 4E**. NR spectra were not drastically changed by the addition of HPOs. However, the data analysis revealed that HPOs always insert into the outer hydrophilic leaflet of the d_{62}DPPC SLB without flipping into the inner layer attached to the silicon block (this is evident from the variation of the external polar leaflet SLD and roughness, as reported in **Figure 4E**). A slight modification of the SLD profiles was observed while adding 13-HPOT but not with 13-HPOD. This gave rise to a small but significant decrease of the membrane thickness (approximately 2 Å) and roughness without modification

of the solvent penetration and of lipid chains SLD, *i.e.*, no alteration of the bilayer nor external molecules deep penetration. To confront these results, obtained on a d_{62}DPPC bilayer, to a more realistic PPM model, another experiment was performed with the deuterated version of 13-HPOD and the ternary mixture of non-deuterated lipids representative of PPM. It confirms that 13-HPOD interacts with PPM SLB and localizes on top of the outer leaflet without no major change of the membrane organization as observed from SLD profile and NR spectra (**Figure S3** and **Table S2**).

3.3.4 Lateral erosion of plant lipid bilayers by HPOs

To further analyse the effect of HPOs on the lipid bilayer organization, atomic force microscopy (AFM) was used to investigate their impact on the lateral nanoscale morphology of SLB. As shown in **Figure 5A**, the ternary mixture of plant lipids reconstituted in SLB did not reveal any phase separation within the thickness resolution limit of AFM (0.1 nm), rather homogeneous smooth patches (bright areas) distributed on the mica (dark areas). Though large patches were mainly found to cover the entire scanned area, defects in the SLB were used as a "visualization control" to confirm the presence of the lipid bilayer. Its thickness of ~4-5 nm, determined by measuring section profiles on the AFM height images, is in agreement with previous studies (**Figure 5B**) (Dufrêne and Lee, 2000; Mingeot-Leclercq *et al.*, 2008). The presence of the lipid bilayer was further confirmed by recording AFM force curves on areas of high *vs* low heights. A typical breakthrough of the lipid bilayer in the bright areas was observed while no such force signature was found in dark areas without lipid bilayers and associated with mica (**Figure 5C**).

After confirming the presence of the SLB, the sample was incubated with either 13-HPOT or 13-HPOD and AFM images were recorded every 10-15 min on a defined area. Incubation 13-HPOT or 13-HPOD resulted in a time-dependent alteration of the lipid patches (**Figure 5D**). Results showed that very small SLB patches (green arrows) disappeared after the addition of 13-HPOT, but that it had not a drastic impact on the large ones. On the contrary, 13-HPOD completely removed part of a large angular domain after 75 min (see

green arrows). Nonetheless, after 75 min treatment with 13-HPOT, most of the lipid domains were thinner by approximately 2 nm as compared to the initial ones, suggesting that 13-HPOT flattened lipids or part of the upper leaflet in a time- and zone-dependent way, which was not observed for 13-HPOD (**Figure 5E-F**).

In brief, AFM studies revealed three major effects of HPOs on plant mimetic lipid bilayers (i) "erosion" of angular protrusions of large lipid domains, (ii) total erosion of small domains, and (iii) reduction in the thickness of the bilayer between 0.5 and 2 nm. 13-HPOT has also a greater effect on membrane organization and bilayer thickness than 13-HPOD.

4 General discussion and conclusion

In the present study, we show for the first time the potential of the exogenous application of acyl-hydroperoxides 13-HPOD and 13-HPOT to protect plants against phytopathogens. Both forms of HPOs applied on *A. thaliana* roots strongly reduce the size of the lesions further to the inoculation of *B. cinerea* on leaves. The protection effect without direct contact with the phytopathogen suggests their capacity to stimulate the plant immune system. Other phyto-oxylipins, such as the jasmonic acid precursor 12-oxo-phytodienoic acid and an α-ketol of octadecadienoic acid were recently identified as mobile signals responsible of ISR, originating in the plant roots and travelling into the plant vasculature (Wang *et al.*, 2020). Our results show that exogenous application of 13-HPOD and 13-HPOT on *A. thaliana* cell suspension induces an important *in vitro* oxidative burst, known as one of the hallmarks of elicitor recognition by plant cells (Yu *et al.*, 2017). Beyond their role as signals, we thus clearly demonstrate that HPOs are recognized by the plant cells and trigger a signalling cascade leading to SR and plant protection against pathogens. However, it remains essential to determine whether other immune responses (such as expression of genes from JA/SA or PTI pathways) are generated in leaves when roots are treated with HPOs. Moreover, we cannot exclude that oxylipins might be transported in the xylem of plants, as traces of oxylipins have been found in aphids' gut after ingestion of phloem sap (Harmel *et al.*, 2007). Nothing is known about the xylem systemicity of oxylipins but, as they are not soluble in water, this

seems unlikely. The possibility that HPOs application in roots just prime the plant immunity in shoots, which initiate stronger immune response when true elicitors from pathogens are perceived, can also not be ruled out. Their effectiveness in the case of a local immune induction is also not known.

The ROS production is initiated later and lasts longer that the one observed with well-known proteic elicitors like flg22 for which recognition phenomenon involves direct interaction with membrane proteic receptors (Gómez-Gómez and Boller, 2002). The late ROS production observed for HPOs could be associated to chloroplasts, like it was shown for lipopolysaccharides and lipid A (Shang-Guan *et al.*, 2018). But the active concentration range is also similar to the one observed for other amphiphilic lipid elicitors like surfactin and RLs (Aranda *et al.*, 2007; Jourdan *et al.*, 2009; Henry *et al.*, 2011; Ma *et al.*, 2017; Luzuriaga-Loaiza *et al.*, 2018) for which a mechanism linked to the perception by the lipid of the plasma membrane was suggested. From our previous work (Deleu *et al.*, 2019), we know that HPOs can interact with the lipid fraction of PPM. In the present study, NR analyses show that both HPOs are more preferably inserted in the outer leaflet of the bilayer. This interaction modifies the global morphology of the bilayer as shown by AFM where bilayer erosion is observed for both HPOs. 13-HPOT has a higher impact on the PPM structure, but does not affect the integrity of the membrane according to the calcein release assays. Its insertion further reduces the thickness of the bilayer according to the NR and AFM data and fluidifies it more than 13-HPOD, according to the Laurdan GP data. This difference between 13-HPOT and 13-HPOD could be explained by the presence of an additional double bond in 13-HPOT which gives it a greater structure rigidity. We postulate that this might force the lipids of the membrane outer leaflet to further reorganize compared to a more flexible molecule like 13-HPOD, and consequently could have a stronger impact on the dynamics of the membrane. The higher binding affinity of 13-HPOT compared to 13-HPOD for PPM bilayer (Deleu *et al.*, 2019) could also enhance this reorganization effect.

The relationship between the higher ROS production and the higher impact on PPM lipid bilayer structure for 13-HPOT compared to 13-HPOD is in favour of our hypothesis that

the PPM lipid fraction plays a key role in the recognition of HPOs giving rise to plant defence mechanisms. In the study of Sandor *et al.* (2016), it is demonstrated on *A. thaliana* and tobacco cells, that the induction of ROS by various elicitors including cryptogein, flg22 and an oligosaccharide, is concomitant to the increase in the relative proportion of membrane ordered domains (Sandor *et al.*, 2016). According to them, the recognition of the elicitor at the plasma membrane level triggers the production of ROS which in turn reorganizes the membrane leading to an increase of ordered domains. But in the case of cryptogein, they have also suggested an inverse event sequence. Although cryptogein is known to trigger immune response, including ROS production, through the PPM-resident ELR-BAK1 receptor complex (Du *et al.*, 2015), its capacity to interact with membrane sterols and to mechanically trap them was also demonstrated (Gerbeau-Pissot *et al.*, 2014). The latter phenomenon was shown to induce a higher membrane fluidity stimulating ROS production (Sandor *et al.*, 2016). In agreement with this study, our results suggest that elicitors that directly act on membrane lipid dynamics and more particularly on the membrane fluidity are able to trigger early defence events like ROS production. But the complete molecular mechanistic view between the change of the membrane structure and the occurrence of the oxidative burst is not yet identified. The formation of specific membrane lipid domains recruiting key signalling proteins (Gronnier *et al.*, 2018) could be implicated. From our previous studies (Deleu *et al.*, 2019; Deboever *et al.*, 2020), we also know that HPOs modify the organisation of lipid domains and that plant membrane sphingolipids are privileged partners for HPO interaction. Therefore, the presence of glycosyl-inositol-phosphoryl-ceramides (GIPCs), the plant sphingolipids exclusively located in the outer leaflet of PPM and involved in the inter-leaflet coupling (Gronnier *et al.*, 2016), could also play a role in the signal transduction.

In addition to their eliciting activity evidenced in the present study, HPOs also retain some antimicrobial activity against various phytopathogens (Deboever *et al.*, 2020). The dual effect of HPOs as well as the possibility to produce them at low cost (Fauconnier and Marlier, 1996) make them attractive compounds to be used as alternative to conventional pesticides for plant protection.

Author Contributions: Experiments design, E.D., M.D., V.R., A.K., M.M.M., M.O. and G.V.A..; experiments and data analysis, E.D., M.D., M.M.M., V.R. and G.V.A.; HPOs synthesis, and purification, E.D.; writing—original draft preparation, E.D.; writing—review and editing, all authors.

Data availability statement: The data supporting the findings of this study are available from the corresponding author, Magali Deleu, upon request.

Funding: E.D. is supported by a « Fonds pour la formation à la Recherche dans l'Industrie et dans l'Agriculture » (FRIA) grant (5100617F) from the FRS-FNRS (Fonds National de la Recherche Scientifique, Belgium). M.D., M. O. and L.L. thank the FRS-FNRS for their position as Senior Research Associates and for grant CDR (J.0014.08 and J.0086.18 projects). Work at the Université Catholique de Louvain was supported by the National Fund for Scientific Research (FNRS) and the Research Department of the Communauté Française de Belgique (Concerted Research Action). Y.F.D. is a Research Director at the FNRS. This research was funded also by the 'Medical Biotechnologies and Translational Medicine Department' of the 'Università degli Studi di Milano', grant number 'PSR2018' to V.R. This article was published with the support of the "Fondation Universitaire de Belgique".

Acknowledgments: The authors thank the financial support via the project from University of Liège (ARC-FIELD project 13/17-10). Authors also thank beamline MARIA Jülich Centre for Neutron Science (JCNS) at Heinz Maier-Leibnitz Zentrum (MLZ, Garching, Germany) for allocation of beamtime. Acknowledgements are also due to FytoFend's research team for their logistic support in bioassays. Final thanks to Jelena Prisc for technical support and nice discussion on ISR and ROS experiment data measured *in planta*.

Conflicts of Interest: EDB, GVA and PVC are members of FytoFend (Belgium). The funders had no role in the design of the study; in the collection, analyses, or interpretation of data; in the writing of the manuscript, or in the decision to publish the results.

5 Figures and Tables

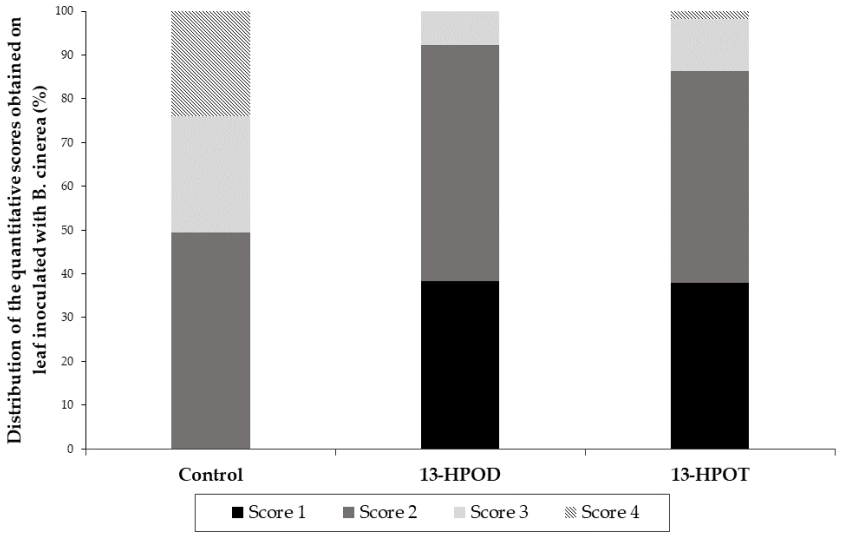

Figure 1 - Disease severity distribution of B. cinerea on leaves from root-treated A. thaliana plants grown hydroponically. Treatments included control and two oxylipins: 13-HPOD and 13-HPOT. Scoring: 1, no symptoms; scoring 2, lesions smaller than 0.5 cm; scoring 3, lesions larger than 0.5 cm; scoring 4, beginning of sporulation on lesions. Results are based on three independent experiments (n=3). Standard deviation between the experiments is less than 7%.

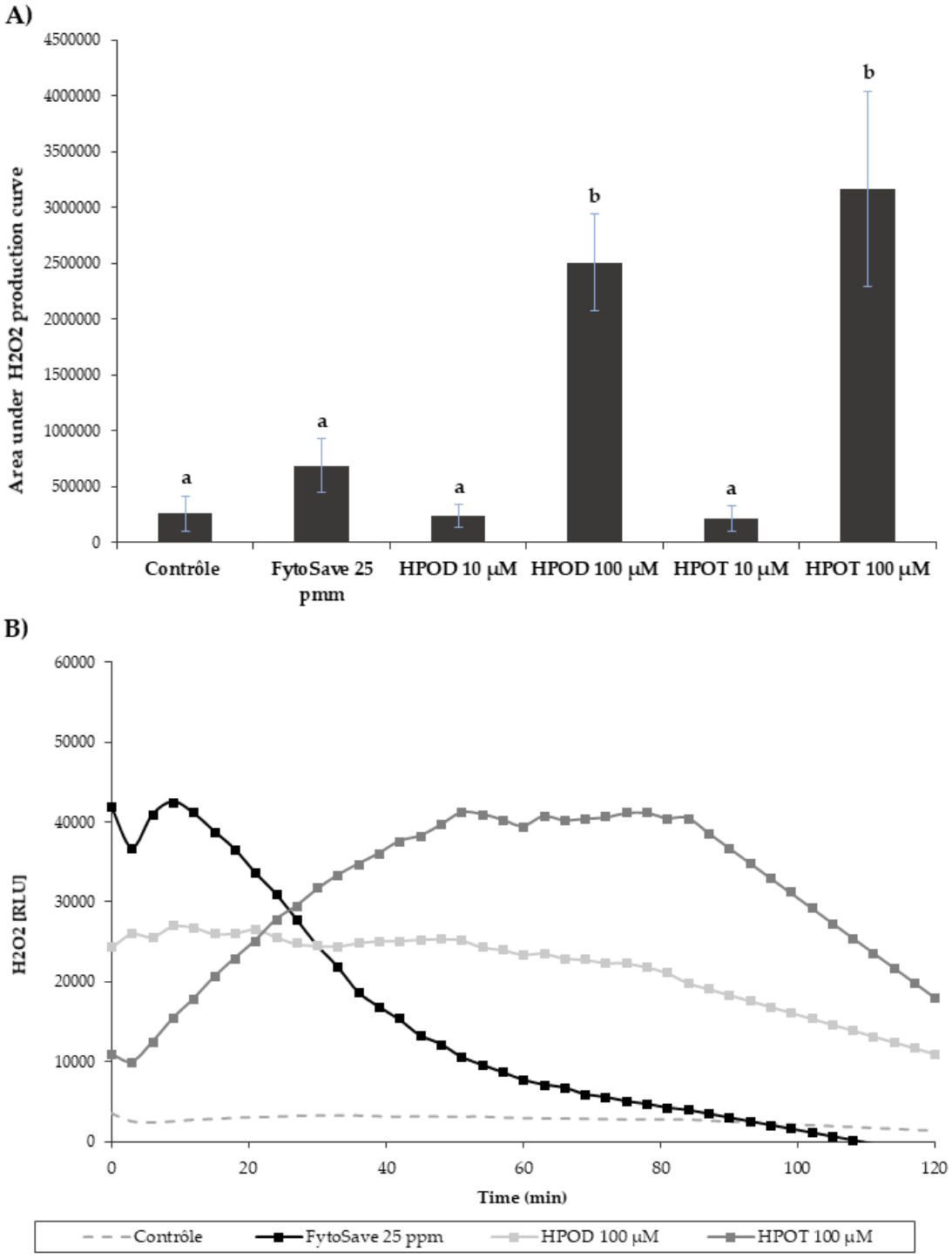

Figure 2 - Early defense responses detection induced by HPOs in *A. thaliana* cells suspensions. **(A, B)** Production of ROS by controls and HPOs treated cells. **(A)** Mean area under H_2O_2 production curves for 90 min measurements. Data are based on three independent repetitions (n=3) and error bars are the standard deviations of means. **(B)** One example of kinetics of ROS production for 13-HPOT, 13-HPOD, MS negative control and COS-OGA positive control.

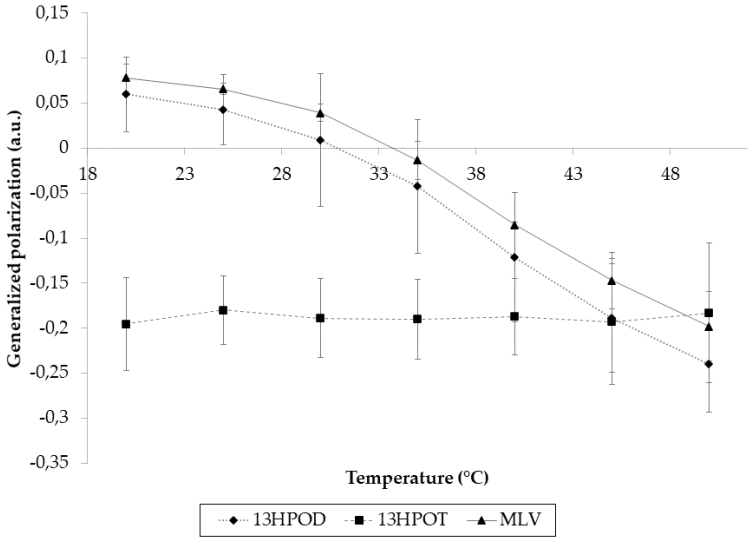

Figure 3 - Evolution of Laurdan generalized polarization as a function of temperature for PLPC:sito:GluCer MLVs (50 µM) in the absence or presence of HPOs (lipid:HPO molar ratio 5:1).

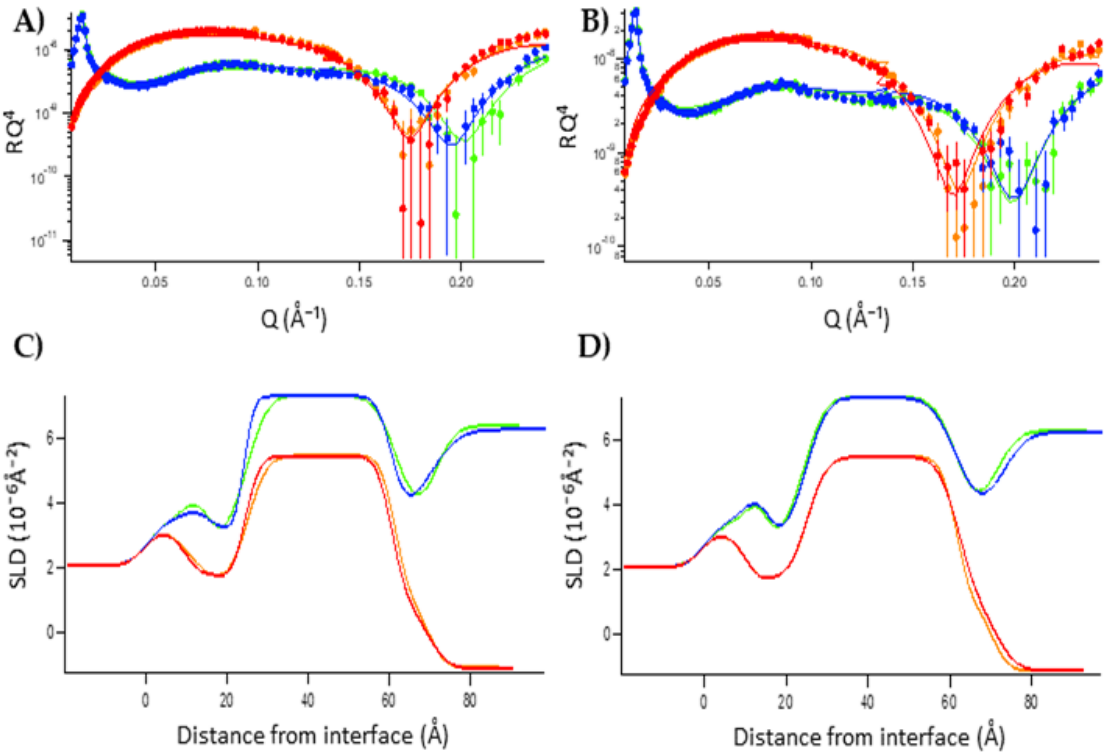

E)

	SLB				SLB + 13-HPOT				SLB + 13-HPOD			
	Thickness (±1 Å)	SLD (±0.05*10⁻⁶Å⁻²)	Solv p (±5% vol)	Roughness (±2 Å)	Thickness (±1 Å)	SLD (±0.05*10⁻⁶Å⁻²)	Solv p (±5% vol)	Roughness (±2 Å)	Thickness (±1 Å)	SLD (±0.05*10⁻⁶Å⁻²)	Solv p (±5% vol)	Roughness (±2 Å)
Solvent	1			5	1			5	1			5
Heads in	10	1,75	32	3	9	1,75	32	4	10	1,75	32	3
Chains in	18	7,66	25	4	17	7,66	25	2	17	7,66	25	4
Chains out	20	766	25	4	19	7,66	25	4	20	7,66	25	4
Heads out	9	1,75	32	4.5	9	1,94	32	3	10	1,87	32	5
		6,36 (D_2O)		4		6,36 (D_2O)		6		6,36 (D_2O)		5
		-0.56 (H_2O)				-0.56 (H_2O)				-0.56 (H_2O)		

Figure 4 - **(A,B)** Reflectivity curves (symbols), relatives fits (lines) and **(C,D)** obtained SLD profiles of the d_{62}DPPC membrane investigated in two contrasts before (green and orange) and after (bleu and red) the addition of 13-HPOT (left) and 13-HPOD (right) (lipid:HPO molar ratio 5:1). **(E)** Fit parameters of the d_{62}DPPC SLB alone and after the interaction with 13-HPOD/T. Parameters (Thickness, scattering length density (SLD), solvent penetration (Solv p) and roughness) correspond to a contemporary fit performed on H_2O and D_2O solutions with 10mM Tris buffer (pH 7.4). Errors have been estimated

by changing the parameters up to a variation of two in the χ^2. For each parameter, the maximum error found was kept. Measurements were carried out at room temperature.

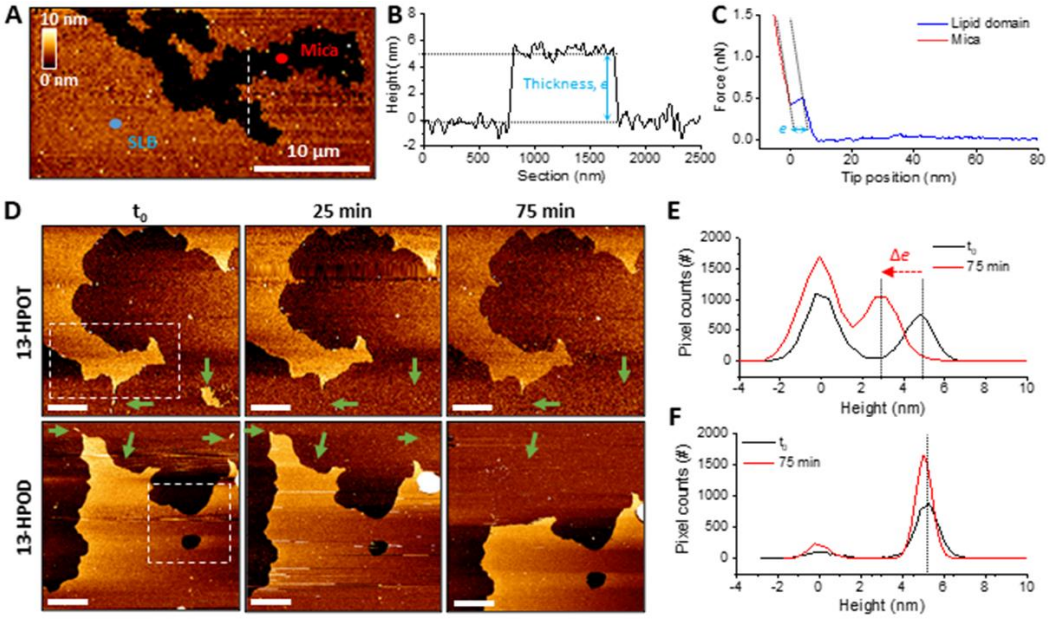

Figure 5 - HPOs lead to lipids erosion. **A)** AFM topographic image of a PLPC:sito:GluCer (60:20:20) supported lipid bilayer (SLB), deposited on mica, and recorded in 10 mM Tris buffer at pH 7.5. **B)** Height profile of the SLB along the dashed line in (A) allowing the measurement of the sample thickness e. **C)** Force curves recorded on a bright area in (A) confirming the presence of the SLB, with a thickness e. **D)** AFM topographic images before (t_0) and after injection of 13-HPOT or 13-HPOD, at increasing incubation times. Scale bar 1 µm, same colour scale than in (A). **E-F)** Height density profiles recorded on small areas, defined as dashed squares in (D), of the PLPC:sito:GluCer bilayer before and after 75 min - incubation with 13-HPOT and 13-HPOD respectively.

Figure S1 - Production of ROS by controls and HPOs treated foliar disks of A. thaliana. Results are expressed as mean ± standard deviation (n = 12) of the area under the H2O2 production curves measured during 120 min. Bars with different letters are statistically different (ANOVA, Tukey's HSD $p < 0.05$).

Table S1 - Theoretical SLD values of the individual chemical species.

Figure S2 - Release of calcein after 900 sec from PLPC:sito:GluCer (60:20:20) liposomes (50 µM), upon addition (at t=30 s) of increasing concentrations of 13-HPOD (dark grey) and 13-HPOT (light grey) in 10 mM Tris-HCl buffer at pH 7,4 and 25°C. The ordinate shows the amount of calcein released in the presence of HPOs as a percentage of the total amount released by 0.2% of Triton X-100.

Figure S3 -– (A) Reflectivity curves (symbols), relatives fits (lines) and (B) obtained SLD profiles of the PLPC:sito:GluCer (60:20:20) membrane investigated in two contrasts before and after the deposition of deuterated 13-HPOD on top of it. Color codes: red, membrane in H2O; orange, membrane in H2O + deuterated 13-HPOD (1x); pink, membrane in H2O + deuterated 13-HPOD (3x); blue, membrane in D2O; green, membrane in D2O deuterated 13-HPOD (1x); turquoise, membrane in D2O deuterated 13-HPOD (3x). Measurements were carried out at room temperature.

Table S2 - Fit parameters of the PLPC:sito:GluCer membrane alone and after addition of 13-HPOD one time concentrated (1x) and 3 times concentrated (3x) at room temperature. Parameters correspond to a contemporary fit performed on H2O and D2O solutions with 10 mM Tris buffer (pH 7.4). Errors have been estimated by changing the parameters up to a variation of two in the $\chi 2$. For each parameter, the maximum error found was kept.

6 References

Aranda FJ, Espuny MJ, Marqués A, Teruel JA, Manresa Á, Ortiz A. 2007. Thermodynamics of the interaction of a dirhamnolipid biosurfactant secreted by Pseudomonas aeruginosa with phospholipid membranes. Langmuir **23**.

van Aubel G, Buonatesta R, Van Cutsem P. 2013. COS-OGA, a new oligosaccharidic elicitor that induces protection against a wide range of plant pathogens. IOBC-WPRS Bulletin **89**, 403–407.

van Aubel G, Cambier P, Dieu M, Van Cutsem P. 2016. Plant immunity induced by COS-OGA elicitor is a cumulative process that involves salicylic acid. Plant Science **247**, 60–70.

van Aubel G, Serderidis S, Ivens J, Clinckemaillie A, Legrève A, Hause B, Van Cutsem P. 2018. Oligosaccharides successfully thwart hijacking of the salicylic acid pathway by Phytophthora infestans in potato leaves. Plant Pathology **67**, 1901–1911.

Bahar O, Mordukhovich G, Luu DD, Schwessinger B, Daudi A, Jehle AK, Felix G, Ronald PC. 2016. Bacterial Outer Membrane Vesicles Induce Plant Immune Responses. Molecular Plant-Microbe Interactions **29**, 374–384.

Baker CJ, Mock NM. 2004. A method to detect oxidative stress by monitoring changes in the extracellular antioxidant capacity in plant suspension cells. Physiological and Molecular Plant Pathology **64**, 255–261.

Bartlett GR. 1958. Calorimetric Assay Phosphorylated for Free Glyceric Acids. Journal of Biological Chemistry **234**, 469–471.

Blée E. 2002. Impact of phyto-oxylipins in plant defense. Trends in Plant Science **7**, 315–321.

Boller T, Felix G. 2009. A Renaissance of Elicitors: Perception of Microbe-Associated Molecular Patterns and Danger Signals by Pattern-Recognition Receptors. Annual Review of Plant Biology **60**, 379–406.

Cabrera J, Boland A, Cambier P, Frettinger P, Van Cutsem P. 2010. Chitosan oligosaccharides modulate the supramolecular conformation and the biological activity of oligogalacturonides in Arabidopsis. Glycobiology **20**, 775–786.

Camejo D, Guzmán-cedeño A, Vera-macias L, Jiménez A. 2019. Oxidative post-translational modi fi cations controlling plant-pathogen interaction. Plant Physiology and Biochemistry **144**, 110–117.

Carvalho FP. 2017. Pesticides, environment, and food safety. Food and Energy Security **6**, 48–60.

Clinckemaillie A, Decroës A, van Aubel G, Carrola dos Santos S, Renard ME, Van Cutsem P, Legrève A. 2017. The novel elicitor COS-OGA enhances potato resistance to late blight. Plant Pathology **66**, 818–825.

Come B, Donato M, Potenza LF, Mariani P, Itri R, Spinozzi F. 2021. The

intriguing role of rhamnolipids on plasma membrane remodelling: From lipid rafts to membrane budding. Journal of Colloid and Interface Science **582**, 669–677.

Deboever E, Deleu M, Mongrand S, Lins L, Fauconnier M-L. 2020. Plant – Pathogen Interactions: Underestimated Roles of Phyto-oxylipins. Trends in Plant Science **25**, 22–34.

Deleu M, Deboever E, Nasir MN, Crowet J-M, Dauchez M, Ongena M, Jijakli H, Fauconnier M-L, Lins L. 2019. Linoleic and linolenic acid hydroperoxides interact differentially with biomimetic plant membranes in a lipid specific manner. Colloids and Surfaces B: Biointerfaces **175**.

Deleu M, Lorent J, Lins L, Brasseur R, Braun N, El Kirat K, Nylander T, Dufrêne YF, Mingeot-Leclercq MP. 2013. Effects of surfactin on membrane models displaying lipid phase separation. Biochimica et Biophysica Acta - Biomembranes **1828**, 801–815.

Du J, Verzaux E, Chaparro-Garcia A, *et al.* 2015. Elicitin recognition confers enhanced resistance to Phytophthora infestans in potato. Nature Plants **1**, 1–5.

Dufrêne YF, Lee GU. 2000. Advances in the characterization of supported lipid films with the atomic force microscope. Biochimica et Biophysica Acta - Biomembranes **1509**, 14–41.

Fauconnier ML, Marlier M. 1996. An efficient procedure for the production of fatty acid hydroperoxides from hydrolyzed flax seed oil and soybean lipoxygenase. Biotechnology Techniques **10**, 839–844.

Fu FN, Singh BR. 1999. Calcein permeability of liposomes mediated by type a botulinum neurotoxin and its light and heavy chains. Journal of Protein Chemistry **18**, 701–707.

Furlan L, Laurin Y, Botcazon C, Rodr N, Buchoux S. 2020. Contributions and Limitations of Biophysical Approaches to Study of the Interactions between Amphiphilic Molecules and the Plant. Plants **9**, 1–24.

Gay H. 2012. Before and after silent spring: From chemical pesticides to biological

control and integrated pest management-Britain, 1945-1980. Ambix **59**, 88–108.

Genva M, Obounou Akong F, Andersson MX, Deleu M, Lins L, Fauconnier ML. 2019. New insights into the biosynthesis of esterified oxylipins and their involvement in plant defense and developmental mechanisms. Phytochemistry Reviews **8**, 343–359.

Gerbeau-Pissot P, Der C, Thomas D, Anca IA, Grosjean K, Roche Y, Perrier-Cornet JM, Mongrand S, Simon-Plas F. 2014. Modification of plasma membrane organization in tobacco cells elicited by cryptogein. Plant Physiology **164**, 273–286.

Gómez-Gómez L, Boller T. 2002. Flagellin perception: A paradigm for innate immunity. Trends in Plant Science **7**, 251–256.

Granér G, Hamberg M, Meijer J. 2003. Screening of oxylipins for control of oilseed rape (Brassica napus) fungal pathogens. Phytochemistry **63**, 89–95.

Gronnier J, Gerbeau-Pissot P, Germain V, Mongrand S, Simon-Plas F. 2018. Divide and Rule: Plant Plasma Membrane Organization. Trends in Plant Science **23**, 899–917.

Gronnier J, Germain V, Gouguet P, Cacas JL, Mongrand S. 2016. GIPC: Glycosyl inositol phospho ceramides, the major sphingolipids on earth. Plant Signaling and Behavior **11**, 1–7.

Haba E, Pinazo A, Pons R, Pérez L, Manresa A. 2014. Complex rhamnolipid mixture characterization and its influence on DPPC bilayer organization. Biochimica et Biophysica Acta - Biomembranes **1838**, 776–783.

Harmel N, Delaplace P, Blée E, Jardin P Du, Fauconnier ML. 2007. Myzus persicae Sulzer aphid contains oxylipins that originate from phloem sap. Journal of Plant Interactions **2**, 31–40.

Harris FM, Best KB, Bell JD. 2002. Use of laurdan fluorescence intensity and polarization to distinguish between changes in membrane fluidity and phospholipid order. Biochimica et Biophysica Acta - Biomembranes **1565**, 123–128.

Henry G, Deleu M, Jourdan E, Thonart P, Ongena M. 2011. The bacterial lipopeptide surfactin targets the lipid fraction of the plant plasma membrane to trigger immune-related defence responses. Cellular Microbiology **13**, 1824–1837.

Henry G, Thonart P, Ongena M. 2012. PAMPs, MAMPs, DAMPs and others: an update on the diversity of plant immunity elicitors. Biotechnologie, Agronomie, Société et … **16**, 12.

Hernández AF, Parrón T, Tsatsakis AM, Requena M, Alarcón R, López-Guarnido O. 2013. Toxic effects of pesticide mixtures at a molecular level: Their relevance to human health. Toxicology **307**, 136–145.

Herzog M, Tiso T, Blank LM, Winter R. 2020. Interaction of rhamnolipids with model biomembranes of varying complexity. Biochimica et Biophysica Acta - Biomembranes **1862**.

Jogaiah S, Govind SR, Shetty HS. 2019. Role of Oomycete Elicitors in Plant Defense Signaling. Bioactive Molecules in Plant Defense. Springer International Publishing, 59–74.

Jourdan E, Henry G, Duby F, Dommes J, Barthélemy JP, Thonart P, Ongena M. 2009. Insights into the defense-related events occurring in plant cells following perception of surfactin-type lipopeptide from Bacillus subtilis. Molecular Plant-Microbe Interactions **22**, 456–468.

Khonon MAR, Okuma E, Hossain MO, Munemasa S, Uraji M, Nakamura Y, Mori IC, Murata Y. 2011. Involvement of extracellular oxidative burst in salicylic acid-induced stomatal closure in Arabidopsis. Plant Cell and Environment **34**, 434–443.

Koutsioubas A. 2016. Combined Coarse-Grained Molecular Dynamics and Neutron Ref ectivity Characterization of Supported Lipid Membranes. The Journal of Physical Chemistry **120**, 11474–11483.

Koutsioubas A, Appavou MS, Lairez D. 2017. Time-Resolved Neutron Reflectivity during Supported Membrane Formation by Vesicle Fusion. Langmuir **33**, 10598–10605.

Lebecque S, Lins L, Dayan FE, Fauconnier M. 2019. Interactions Between Natural Herbicides and Lipid Bilayers Mimicking the Plant Plasma Membrane. Frontiers in Pharmacology **10**, 1–11.

Ledoux Q, Van Cutsem P, Markó IE, Veys P. 2014. Specific localization and

measurement of hydrogen peroxide in Arabidopsis thaliana cell suspensions and protoplasts elicited by COS-OGA. Plant Signaling & Behavior **9**, 1–6.

Luzuriaga-Loaiza WP, Schellenberger R, De Gaetano Y, *et al.* 2018. Synthetic Rhamnolipid Bolaforms trigger an innate immune response in Arabidopsis thaliana. Scientific Reports **8**, 1–13.

Ma Z, Ongena M, Höfte M. 2017. The cyclic lipopeptide orfamide induces systemic resistance in rice to Cochliobolus miyabeanus but not to Magnaporthe oryzae. Plant Cell Reports **36**, 1731–1746.

Malik ANA, Kumar IS, Nadarajah K. 2020. Elicitor and Receptor Molecules: Orchestrators of Plant Defense and Immunity. International Journal of Molecular Sciences **21**, 963–997.

Mattauch S, Koutsioubas A, Ru U, *et al.* 2018. The high-intensity reflectometer of the Jülich Centre for Neutron Science: MARIA research papers. Journal of Applied Cristallography **51**, 1–9.

Meindl T, Boller T, Felix G. 2000. The bacterial elicitor flagellin activates its receptor in tomato cells according to the address-message concept. Plant Cell **12**, 1783–1794.

Mingeot-Leclercq MP, Deleu M, Brasseur R, Dufrêne YF. 2008. Atomic force microscopy of supported lipid bilayers. Nature Protocols **3**, 1654–1659.

Mittler R. 2017. ROS Are Good. Trends in Plant Science **22**, 11–19.

Monnier N, Furlan A, Botcazon C, Dahi A, Mongelard G, Cordelier S, Clément C, Dorey S, Sarazin C, Rippa S. 2018. Rhamnolipids From Pseudomonas aeruginosa Are Elicitors Triggering Brassica napus Protection Against Botrytis cinerea Without Physiological Disorders. Frontiers in Plant Science **9**, 1–14.

Nelson A. 2006. Co-refinement of multiple-contrast neutron / X-ray reflectivity data using MOTOFIT. Journal of Applied Cristallography **39**, 273–276.

Névot L, Croce P. 1980. Caractérisation des surfaces par réflexion rasante de rayons X. Application à l'étude du polissage de quelques verres silicates. Revue de Physique Appliquée **15**, 761–779.

Ngou BPM, Ahn HK, Ding P, Jones JDG. 2021*a*. Mutual potentiation of plant immunity by cell-surface and intracellular receptors. Nature **592**, 110–115.

Ngou BPM, Jones JDG, Ding P. 2021*b*. Plant immune networks. Trends in Plant Science, 1–19.

Nimchuk Z, Eulgem T, Holt BF, Dangl JL. 2003. Recognition and Response in the Plant Immune System. Annual Review of Genetics **37**, 579–609.

Nishad R, Ahmed T, Rahman VJ, Kareem A. 2020. Modulation of Plant Defense System in Response to Microbial Interactions. Frontiers in Microbiology **11**, 1–13.

Ongena M, Daayf F, Jacques P, Thonart P, Benhamou N, Paulitz TC, Bélanger RR. 2000. Systemic induction of phytoalexins in cucumber in response to treatments with fluorescent pseudomonads. Plant Pathology **49**, 523–530.

Ongena M, Jourdan E, Adam A, Paquot M, Brans A, Joris B, Arpigny JL, Thonart P. 2007. Surfactin and fengycin lipopeptides of Bacillus subtilis as elicitors of induced systemic resistance in plants. Environmental Microbiology **9**, 1084–1090.

Parasassi T, Gratton E. 1995. Membrane lipid domains and dynamics as detected by Laurdan fluorescence. Journal of Fluorescence **5**, 59–69.

Parasassi T, De Stasio G, Ravagnan G, Rusch RM, Gratton E. 1991. Quantitation of lipid phases in phospholipid vesicles by the generalized polarization of Laurdan fluorescence. Biophysical Journal **60**, 179–189.

Parasassi T, Di Stefano M, Ravagnan G, Sapora O, Gratton E. 1992. Membrane aging during cell growth ascertained by laurdan generalized polarization. Experimental Cell Research **202**, 432–439.

Paré PW, Farag MA, Krishnamachari V, Zhang H, Ryu CM, Kloepper JW. 2005. Elicitors and priming agents initiate plant defense responses. Photosynthesis Research **85**, 149–159.

Prost I, Dhondt S, Rothe G, *et al.* 2005. Evaluation of the Antimicrobial Activities of Plant Oxylipins Supports Their Involvement in Defense against Pathogens. Plant Physiology **139**, 1902–1913.

Pršić J, Ongena M. 2020. Elicitors of Plant Immunity Triggered by Beneficial Bacteria. Frontiers in Plant Science **11**, 1–12.

Rondelli V, Brocca P, Motta S, Messa M, Colombo L, Salmona M, Fragneto G, Cantu L, Del Favero E. 2016. Amyloidβ Peptides in interaction with raft-mime model membranes: A neutron reflectivity insight. Scientific Reports **6**, 1–11.

Rondelli V, Cola E Di, Koutsioubas A, Alongi J, Ferruti P, Ranucci E, Brocca P. 2019. Mucin Thin Layers: A Model for Mucus-Covered Tissues. International Journal of Molecular Sciences **20**, 1–15.

Rondelli V, Del Favero E, Brocca P, *et al.* 2018. Directional K + channel insertion in a single phospholipid bilayer: Neutron reflectometry and electrophysiology in the joint exploration of a model membrane functional platform. Biochimica et Biophysica Acta - General Subjects **1862**, 1742–1750.

Sanchez SA, Tricerri MA, Gunther G, Gratton E. 2007. Laurdan Generalized Polarization: from cuvette to microscope. Modern Research and Educational Topics in Microscopy, 1007–1014.

Sandor R, Der C, Grosjean K, Anca I, Noirot E, Leborgne-Castel N, Lochman J, Simon-Plas F, Gerbeau-Pissot P. 2016. Plasma membrane order and fluidity are diversely triggered by elicitors of plant defence. Journal of Experimental Botany **67**, 5173–5185.

Sautrey G, Zimmermann L, Deleu M, Delbar A, Machado LS, Jeannot K, Van Bambeke F, Buyck JM, Decout JL, Mingeot-Leclercq MP. 2014. New amphiphilic neamine derivatives active against resistant Pseudomonas aeruginosa and their interactions with lipopolysaccharides. Antimicrobial Agents and Chemotherapy **58**, 4420–4430.

Schellenberger R, Crouzet J, Nickzad A, *et al.* 2021. The bacterial virulence factors rhamnolipids and their (R)-3-hydroxyalkanoate precursors activate Arabidopsis innate immunity through two independent mechanisms. bioRxiv.

Schellenberger R, Touchard M, Clément C, Baillieul F, Cordelier S, Crouzet J, Dorey S. 2019. Apoplastic invasion patterns triggering plant immunity: plasma membrane sensing at the frontline. Molecular Plant Pathology **20**, 1602–1616.

Shang-Guan K, Wang M, Htwe NMPS, *et al.* 2018. Lipopolysaccharides trigger two successive bursts of reactive oxygen species at distinct cellular locations. Plant Physiology **176**, 2543–2556.

Shimanouchi T, Ishii H, Yoshimoto N, Umakoshi H, Kuboi R. 2009. Calcein permeation across phosphatidylcholine bilayer membrane: Effects of membrane fluidity, liposome size, and immobilization. Colloids and Surfaces B: Biointerfaces **73**, 156–160.

Smith JM, Heese A. 2014. Rapid bioassay to measure early reactive oxygen species production in Arabidopsis leave tissue in response to living Pseudomonas syringae. Plant Methods **10**, 1–9.

Song W, Forderer A, Yu D, Chai J. 2021. Structural biology of plant defence. New Phytologist **229**, 692–711.

Thakur M, Sohal BS. 2013. Role of Elicitors in Inducing Resistance in Plants against Pathogen Infection: A Review. ISRN Biochemistry **2013**, 1–10.

Wang K Der, Borrego EJ, Kenerley CM, Kolomiets M V. 2020. Oxylipins Other Than Jasmonic Acid Are Xylem-Resident Signals Regulating Systemic Resistance Induced by Trichoderma virens in Maize. The Plant cell **32**, 166–185.

Wang S, Wang Z, Zhang Y, Wang J, Guo R. 2013. Pesticide residues in market foods in Shaanxi Province of China in 2010. Food Chemistry **138**, 2016–2025.

Wasternack C, Feussner I. 2018. The Oxylipin Pathways: Biochemistry and Function. Annual Review of Plant Biology **69**, 363–386.

Wasternack C, Strnad M. 2018. Jasmonates: News on Occurrence, Biosynthesis, Metabolism and Action of an Ancient Group of Signaling Compounds. International Journal of Molecular Sciences **19**, 2539.

Yu X, Feng B, He P, Shan L. 2017. From Chaos to Harmony: Responses and Signaling upon Microbial Pattern Recognition. Annual Review of Phytopathology **55**, 109–137.

Zaid A, Wani SH. 2019. Reactive Oxygen Species Generation, Scavenging and Signaling in Plant Defense Responses. Bioactive Molecules in Plant Defense. Springer

International Publishing, 111–132.

Zhao JL, Zhou LG, Wu JY. 2010. Effects of biotic and abiotic elicitors on cell growth and tanshinone accumulation in Salvia miltiorrhiza cell cultures. Applied Microbiology and Biotechnology **87**, 137–144.